Supporting Information

# Impact of Free Valence Electrons Contraction on Nanoclusters Optical and Electrocatalytic Properties: based on $M_1Ag_{14}$ (M = Pt/Pd) Series Nanoclusters

**Tingting Liu,[b] Yuansheng Li,[b] Yang Zuo,[b] Along Ma,[a] Yifei Wang,[b] Shuo Zhang,[b] Xiaoshuang Ma,[b] Zhengmao Yin,*[b] Junxian Yang*[b] and Shuxin Wang*[a]**

Along Ma, Shuxin Wang*
College of Chemistry and Molecular Engineering, Qingdao University of Science and Technology, Qingdao 266042, China.
email: shuxin_wang@qust.edu.cn

Tingting Liu, Yuansheng Li, Yang Zuo, Shuo Zhang, Yifei Wang, Shuo Zhang, Xiaoshuang Ma, Zhengmao Yin*, Junxian Yang*
College of Materials Science and Engineering, Qingdao University of Science and Technology, Qingdao 266042, China.
email: yzm198752@163.com, yangjx@qust.edu.cn

# Table of Contents

# Section 1. Characterization, Electrochemical measurements, and DTF calculations

## I. Characterization

**Ultraviolet-visible spectroscopy** (**UV-Vis**): The UV-Vis spectra were acquired using a Shanghai Metash UV-8000 spectrophotometer. All the samples were dissolved in $CH_2Cl_2$ for the spectral measurements.

**X-ray photoelectron spectroscopy** (**XPS**): The XPS measurements were carried out using an ESCALAB XI+ system equipped with a monochromated AlKα (1486.8 eV) 150W X-ray source, a 0.5 mm circular spot, and a flood gun to mitigate charging effects. The base pressure in the analysis chamber was maintained below 1 x $10^{-9}$ mbar, and data were collected with a pass energy of 20 eV. The crystal particles of $\mathbf{Pd_1Ag_{14}}$ and $\mathbf{Pt_1Ag_{14}}$ were adhered to packaging tape for testing, with a small amount of carbon added for data correction.

**Scanning electron microscope-energy dispersive spectrometer** (**SEM-EDS**): SEM-EDS analysis was performed using a JSM-6700F instrument. The crystal particles of $\mathbf{Pd_1Ag_{14}}$ and $\mathbf{Pt_1Ag_{14}}$ were mounted on conductive adhesive, and the measurements were taken with an accelerating voltage ranging from 0.1 to 30 kV.

**Thermogravimetric analysis** (**TGA**): TGA was performed using a thermogravimetric analyzer (DTG-60H) with approximately 8 mg of nanoclusters placed in a $SiO_2$ pan. The analysis was conducted at a heating rate of 20 K/min under a nitrogen atmosphere. Prior to TGA testing, the sample was extracted for 5 hours with a vacuum pump to eliminate solvent molecules.

**Nuclear magnetic resonance** (**NMR**): NMR measurements were performed using a Bruker Avance spectrometer operating at 400 MHz for $^1H$. For the preparation sample, electrolysis was performed at each potential from -0.9 V (vs. RHE) to -1.7 V (vs. RHE) for 8 minutes. After 400 μL of the cathode reaction solution and 200 μL of $D_2O$ (using DMSO as an internal standard) were mixed, $^1H$ NMR tests were performed directly.

**X-ray crystallography:**

The data collections for single crystal X-ray diffraction (SC-XRD) were carried out on a Bruker D8 Quest at 170 K, using Mo-Kα radiation (λ = 0.71073 Å). The structure was solved by intrinsic phasing and refined with full-matrix least squares on $F^2$ using the SHELXTL software package. All non-hydrogen atoms were refined anisotropically, and all the hydrogen atoms were set in geometrically calculated positions and refined isotopically using a riding model. Detailed crystal data for $\mathbf{Pt_1Ag_{14}}$ nanocluster is given in Table S1. The CCDC number for $\mathbf{Pt_1Ag_{14}}$ is 2413566, which includes the supplementary crystallographic data associated with this study. These data are provided free of charge by the Cambridge Crystallographic Data Centre.

## II. Electrochemical measurements

To prepare the catalyst sample, the as-prepared two $\mathbf{M_1Ag_{14}}$ nanoclusters were loaded on Multi-walled Ketjen Carbon (C) with a mass ratio of 1 (5 mg nanoclusters and 5 mg Ketjen Carbon). The catalyst ink was prepared by dispersing the sample in isopropanol (2.5 mg·mL$^{-1}$) under sonication for 20 minutes. Then, 1 mL catalyst suspension and 10 μL Nafion (5 wt.%) were uniformly mixed

as the final catalyst ink. Subsequently, 40 μL catalytic ink was dropwise cast onto the carbon cloth (1 × 1 $cm^2$) and dried at room temperature as the working electrode. 0.5 M $KHCO_3$ solution (pH = 7.2 when saturated with $CO_2$) was used as the electrolyte.

The electrochemical properties of two catalysts were evaluated on a DONGHUA DH7001B electrochemical workstation. All electrochemical measurements were carried out in a custom gas-tight H-cell with two compartments separated by Nafion 117 membrane. Each compartment contained 25 mL electrolyte (0.5 M $KHCO_3$) with approximately 10 mL headspace. Ag/AgCl in 0.5 M $KHCO_3$ saturated aqueous electrolyte was employed as the reference electrode. Electrode potentials measured on the Ag/AgCl scale ($E_{Ag/AgCl}$) were converted into the reversible hydrogen electrode (RHE) scale using the following equation:

$E(RHE) = E(Ag/AgCl) + 0.1976 + 0.0592 \times pH$

The output of the gas flow from the cathode chamber passes through a gas flow controller (the gas flow controller was used to control the gas flow rate) and then into a gas chromatograph instrument (GC3900Plus, RUI NENG) for on-line identification and quantification of the gaseous products, which was purged for 30 min with an average rate of 10 $mL \cdot min^{-1}$ (at room temperature and ambient pressure) prior to the test.

The faradaic efficiency ($FE_X$) and partial current density ($j_X$) of X (X= CO or $H_2$) were calculated as below:

$$FE_X = \frac{(N_i \times n \times F)}{Q_t}$$

$$j_X = \frac{FE_X \times Q_t}{t \times \text{Area}}$$

Where

$Q_t$ = total charge consumed in the electrochemical reaction

$N_i$ = the number of moles of the product (measured GC)

$n$ = the number of electrons transferred in the elementary reaction (n is 2 for CO and $H_2$)

$F$ = the Faradaic constant (96485 C $mol^{-1}$)

$t$ = reaction time (s)

Area = geometry area of the electrode (1 $cm^2$)

An Ag/AgCl electrode containing 3.4 $mol \cdot L^{-1}$ KCl was used as the reference electrode, a 1 × 1 $cm^2$ platinum plate served as the counter electrode, and a catalyst-coated carbon cloth was employed as the working electrode. The ECSA was determined in a 0.5 M $KHCO_3$ electrolyte using cyclic voltammetry (CV) curves recorded over a potential range of 0.2 to 0.3 V (vs. RHE) at scan rates ranging from 20 to 100 $mV \cdot s^{-1}$. All CV curves were obtained during $CO_2$ electroreduction without IR compensation. The current density showed a linear relationship with the scan rate, and its proportionality constant corresponds to the double-layer capacitance ($C_{dl}$). The ECSA was calculated using the following formula:

$$ECSA = \frac{C_{dl}}{C_s}$$

$C_{dl}$ = the measured electric double-layer capacitance

$C_s$ = the specific capacitance of the electrode material.

After the $eCO_2RR$ tests were completed, the samples were rinsed with $CH_2Cl_2$ and collected for UV-vis characterization.

At each potential, 400 μL of the electrolyzed catholyte was collected, and 200 μL of $D_2O$ containing DMSO as an internal standard was added. The product peak area was calculated using MestReNova, and the Faraday efficiency ($FE_{formate}$) of the liquid product was calculated using the following formula:

$$n_{formate} = \frac{n_{DMSO} \times n_1 \times S_1}{n_2 \times S_2}$$

$$FE_{formate} = \frac{n_{foemate} \times F \times n}{Q_t \times n_3} \times 100\%$$

Where

$n_{Dmso}$ = The amount of the substance of the internal standard DMSO (0.00063mmol).

$n$ = the number of electrons transferred in the elementary reaction (n is 2 for formare).

$n_1$ = Amount of methyl ($-CH_3$) hydrogen on dimethyl sulfoxide ($n_1 = 6$).

$n_2$ = The amount of carboxyl (-COOH) hydrogen on formate ($n_2 = 1$).

$n_3$ = The ratio of cathode reaction solution to total catholyte taken when configuring $^1H$ NMR ($n_3 = 0.016$).

$S_1$ = MestReNova calculates the HCOOH peak area based on the DMSO peak area.

$S_2$ = The DMSO peak area in MestReNova is set to 1.

$F$ = the Faradaic constant (96485 C $mol^{-1}$).

$Q_t$ = total charge consumed in the electrochemical reaction.

## III. DFT calculations

Periodic DFT calculations were performed with the VASP code using the Perdew-Burke-Ernzerhof exchange-correlation function of the generalized gradient approximation (GGA). Projector augmented wave (PAW) pseudopotential was used to describe core-valence interactions, with [Pt]-$6s^15d^9$, [Pd]-$4d^{10}$ and [Ag]-$5s^14d^{10}$ as valence electrons. The plane-wave cutoff energy was set to 400 eV. The Brillouin zone of the reciprocal space was sampled with the Γ-centred Monkhorst-Pack scheme, the k-point mesh was set to 1 × 1 × 1 for the geometry optimization. The energy convergence of the self-consistent iteration reached $10^{-5}$ eV per atom and the Hellmann-Feynman forces convergence was 0.03 eV $Å^{-1}$, ensuring that the structure optimization process converged to a stable structure.

## Section 2. Supporting Figures

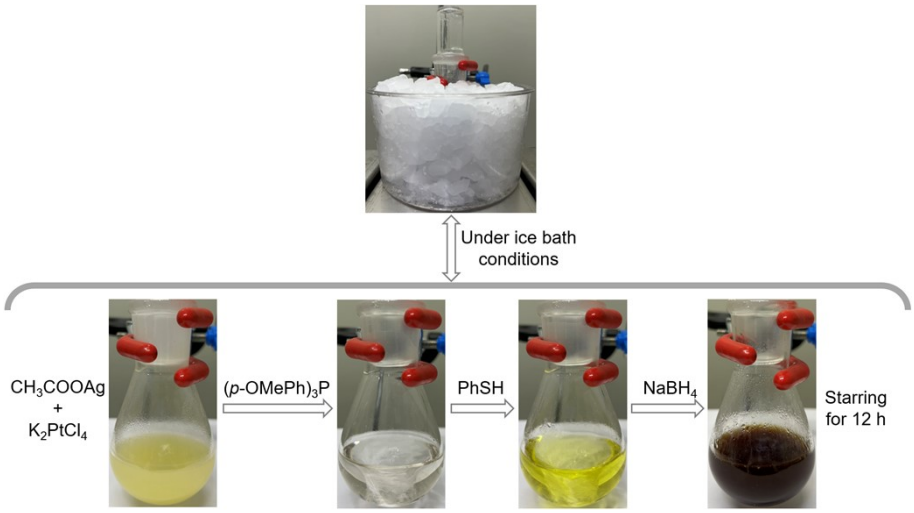


**Scheme S1.** Photographs of the synthesis process of the **$Pt_1Ag_{14}$** nanocluster. The entire reaction was carried out under ice bath conditions; however, to capture clear images of the reaction, the reaction mixtures were temporarily removed from the ice bath during photography.

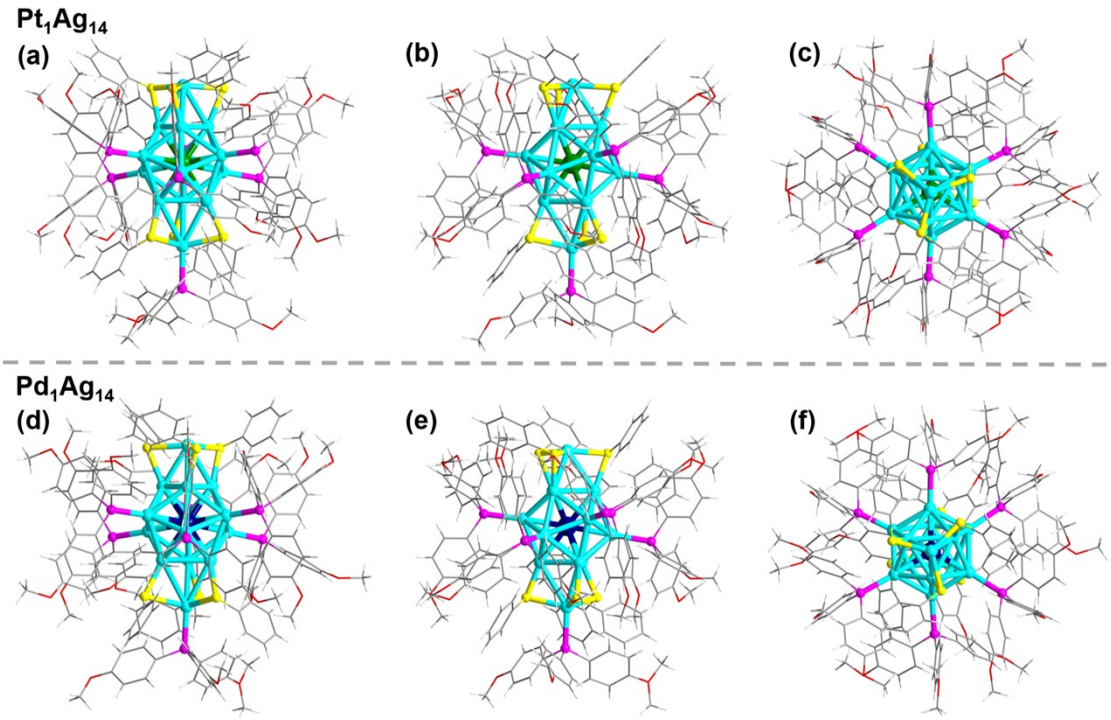


**Fig. S1** The overall structure of the **$Pt_1Ag_{14}$** and **$Pd_1Ag_{14}$** nanoclusters. The (a) front view, (b) top view, and (c) top view of the **$Pt_1Ag_{14}$** nanocluster; The (d) front view, (e) side view, and (f) top view of the **$Pd_1Ag_{14}$** nanocluster. Color labels: green = Pt; dark blue = Pd; light blue = Ag; yellow = S; magenta = P; red = O; grey = C; white = H.

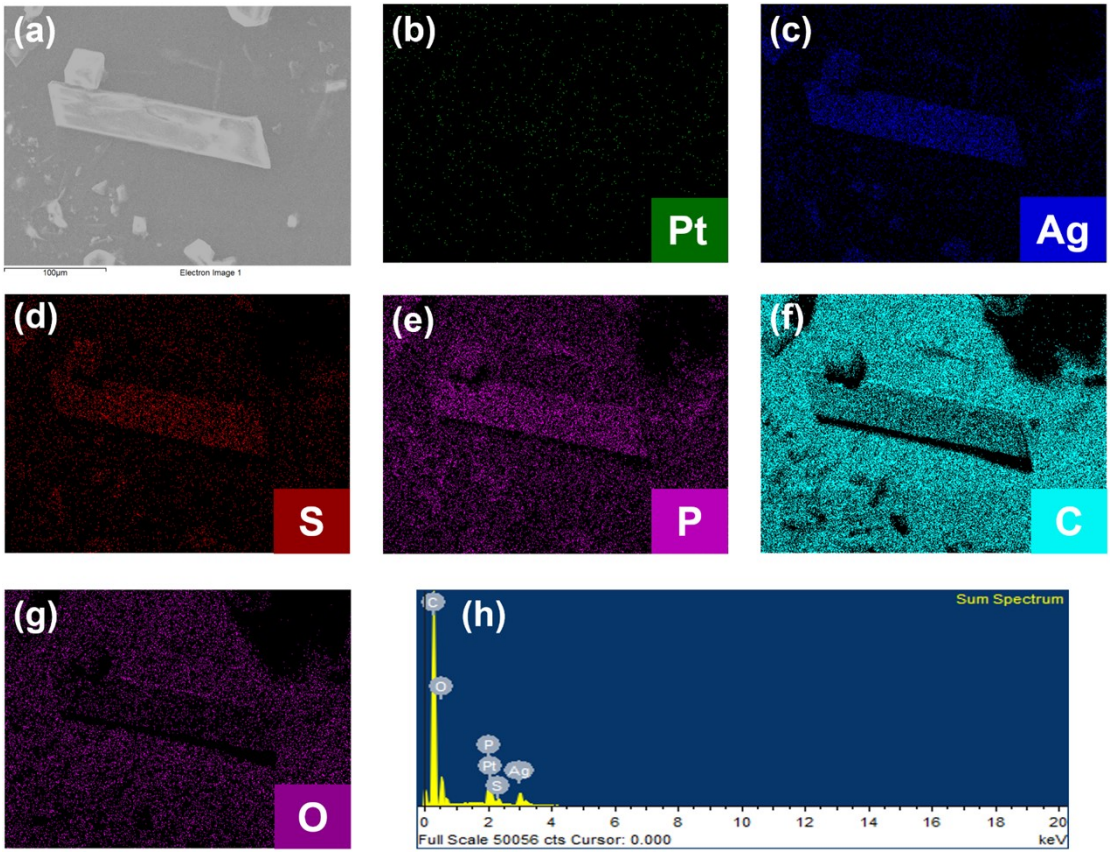


**Fig. S2** SEM image and corresponding elemental mapping images of the $\mathbf{Pt_1Ag_{14}}$ nanocluster. (a) SEM image of single crystal; (b)-(g) elemental mapping images of Pt, Ag, S, P, C and O elements, respectively; (h) EDS spectrum confirming the presence of above elements (Pt, Ag, S, P, C and O) in $\mathbf{Pt_1Ag_{14}}$ nanocluster, which is consistent with the cluster composition obtained by SC-XRD.

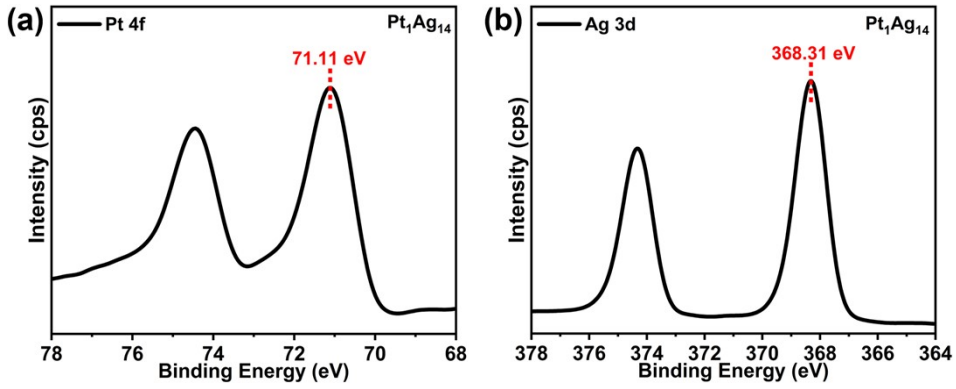


**Fig. S3** XPS spectra of the $\mathbf{Pt_1Ag_{14}}$ nanocluster. (a) Pt 4f; (b) Ag 3d.

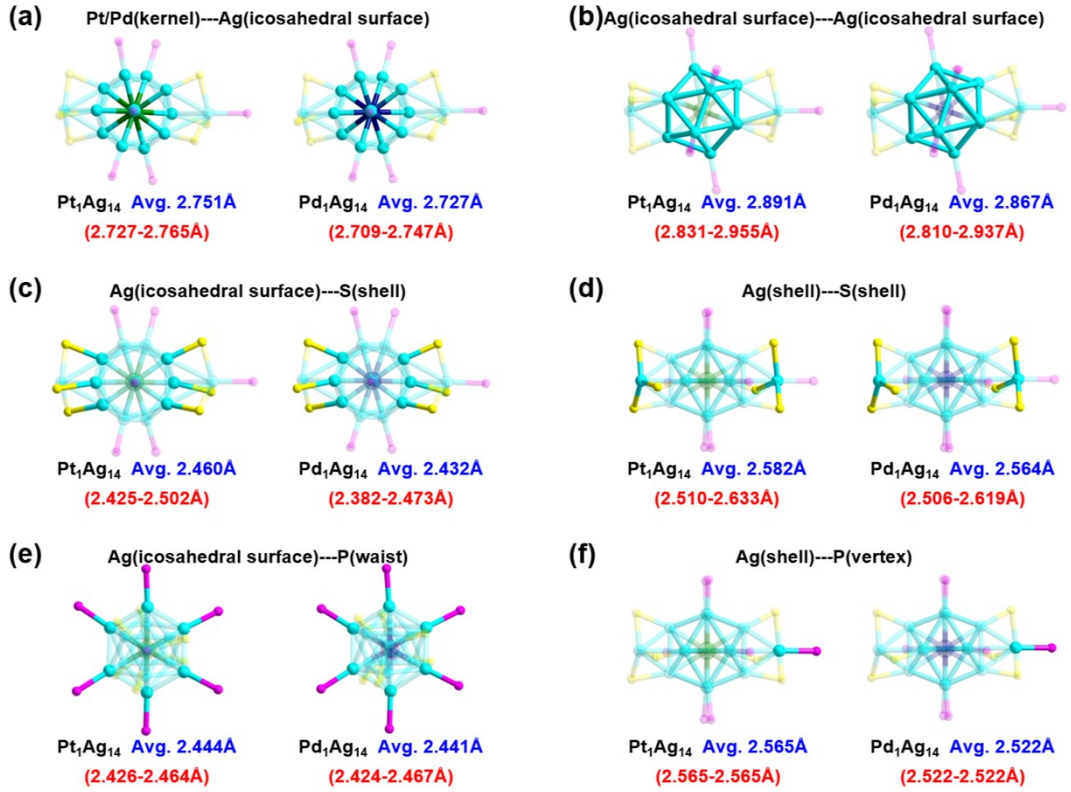


**Fig. S4** Structural comparison and bond length among $\mathbf{Pt_1Ag_{14}}$ and $\mathbf{Pd_1Ag_{14}}$ nanoclusters. (a) Comparison of the bond length of Pt/Pd(kernel)---Ag(icosahedral surface); (b) comparison of the bond length of Ag(icosahedral surface)---Ag(icosahedral surface); (c) comparison of the bond length of Ag(icosahedral surface)---S(shell); (d) comparison of the bond length of Ag(shell)---S(shell); (e) comparison of the bond length of Ag(icosahedral surface)---P(waist); (f) comparison of the bond length of Ag(shell)---P(vertex). The compared bonds are highlighted in solid. Color labels: green = Pt; dark blue = Pd; light blue = Ag; yellow = S; magenta = P.

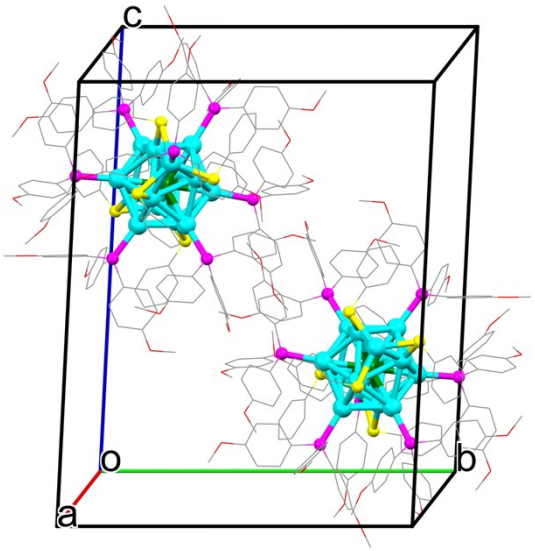


**Fig. S5** A unit cell in the $\mathbf{Pt_1Ag_{14}}$ single crystal. Color labels: green = Pt; light blue = Ag; yellow = S; magenta = P; red = O; grey = C. All H atoms are omitted for clarity.

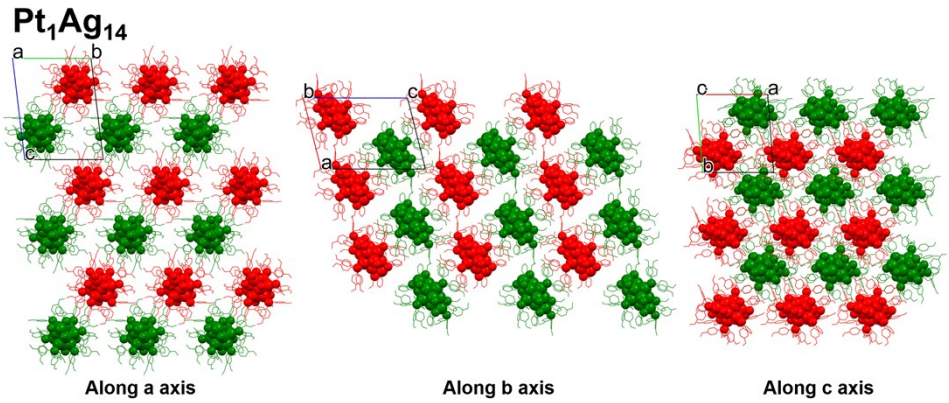


**Fig. S6** Packing mode of $Pt_1Ag_{14}$ in the crystal shown. (a) Along a axis; (b) along b axis; (c) along c axis. All H atoms are omitted for clarity. The cluster molecules arranged in different directions show in different colors.

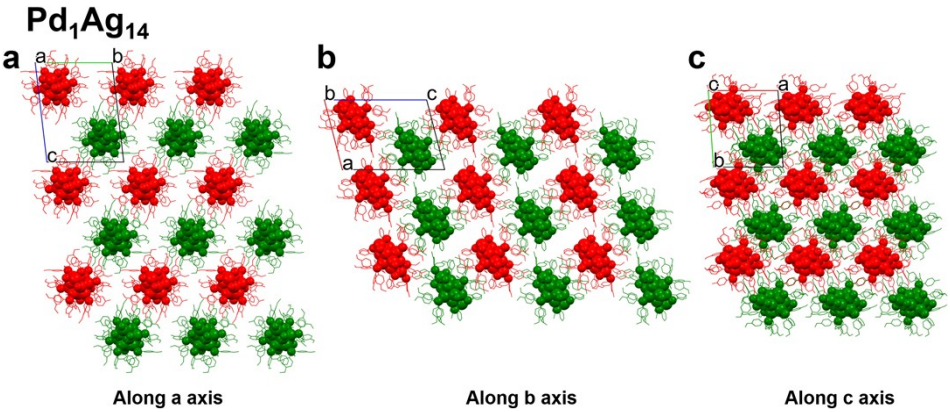


**Fig. S7** Packing mode of $Pd_1Ag_{14}$ in the crystal shown. (a) Along a axis; (b) along b axis; (c) along c axis. All H atoms are omitted for clarity. The cluster molecules arranged in different directions show in different colors.

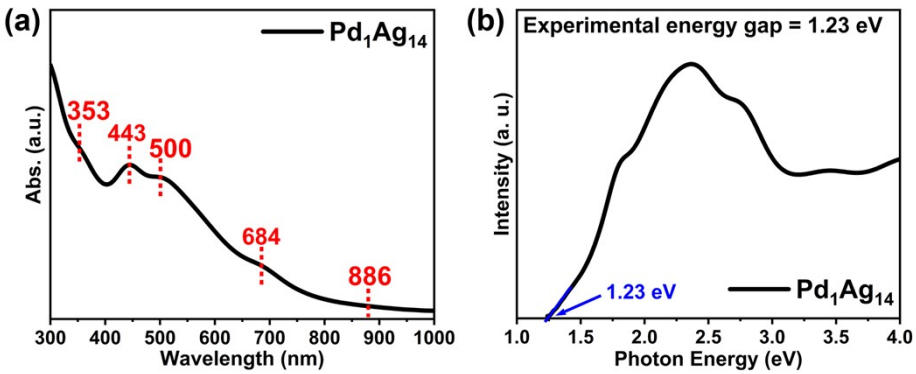


**Fig. S8** Characterization of $Pd_1Ag_{14}$ nanocluster. (a) UV-Vis spectrum; (b) UPS.

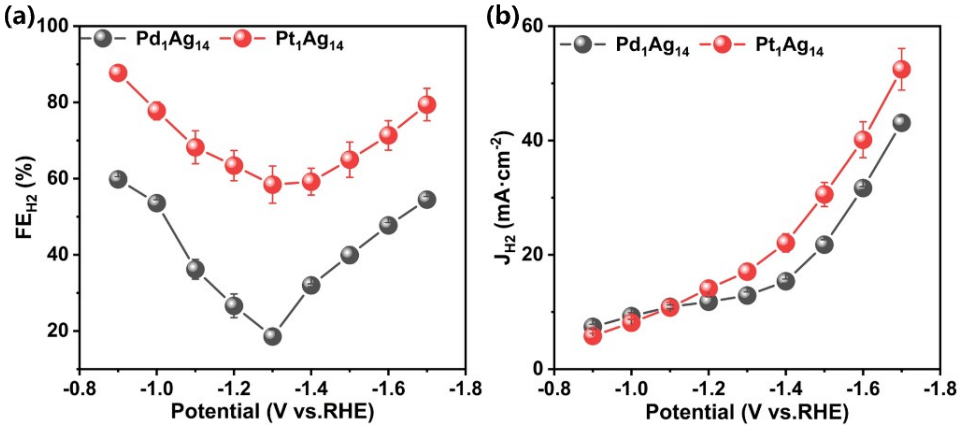


**Fig. S9** (a) $H_2$ faradaic efficiency of the **$Pd_1Ag_{14}$/C** (black) and **$Pt_1Ag_{14}$/C** (red) at different potentials. (b) $H_2$ partial current density of the **$Pd_1Ag_{14}$/C** (black) and **$Pt_1Ag_{14}$/C** (red) at different potentials.

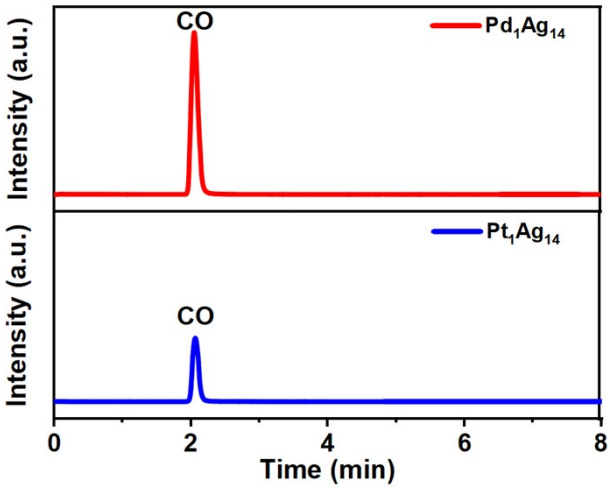


**Fig. S10** Gas products (CO) analysis for $eCO_2RR$ on **$Pd_1Ag_{14}$/C** and **$Pt_1Ag_{14}$/C**. Gas chromatography shows the gas products of $eCO_2RR$ at –1.3 $V_{RHE}$.

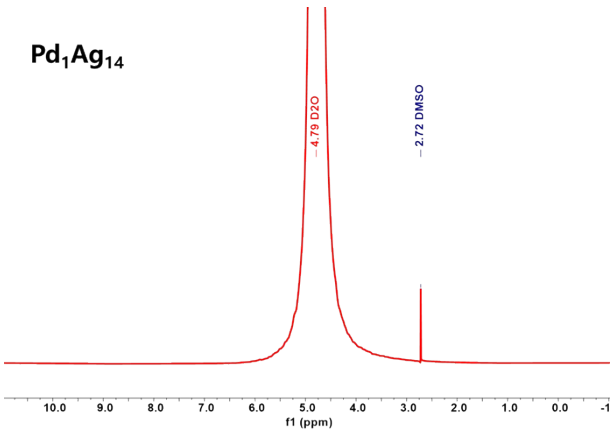


**Fig. S11** The $^1H$ NMR spectra of the catholyte reaction solution for the **$Pd_1Ag_{14}$/C**.

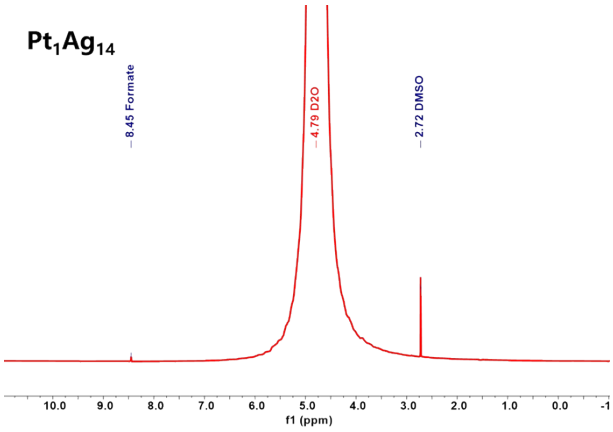


**Fig. S12** The $^{1}$H NMR spectra of the catholyte reaction solution for the **$Pt_1Ag_{14}$/C**.

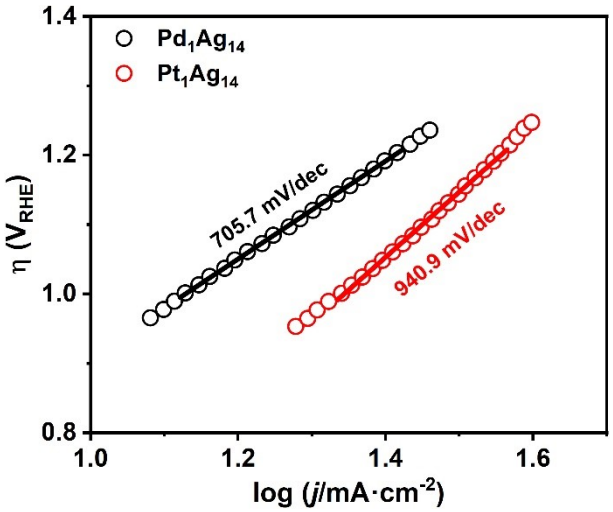


**Fig. S13** Tafel plots constructed for the $eCO_2RR$ on the two catalysts.

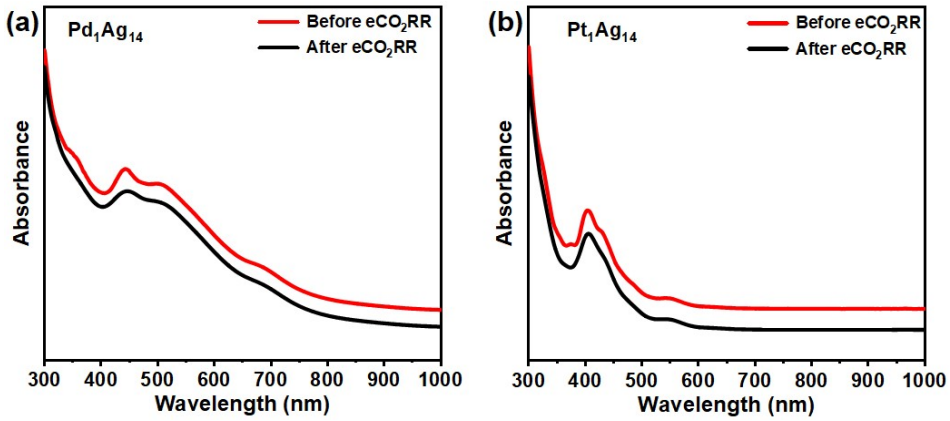


**Fig. S14** UV-vis absorbance spectra of the three nanoclusters before and after $eCO_2RR$. (a) **$Pd_1Ag_{14}$** and (b) **$Pt_1Ag_{14}$**.

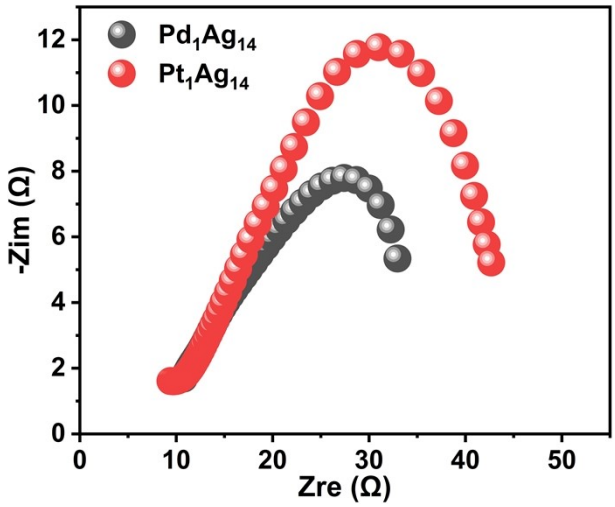


**Fig. S15** The Electrochemical Impedance Spectroscopy of **$Pd_1Ag_{14}$/C** and **$Pt_1Ag_{14}$/C**.

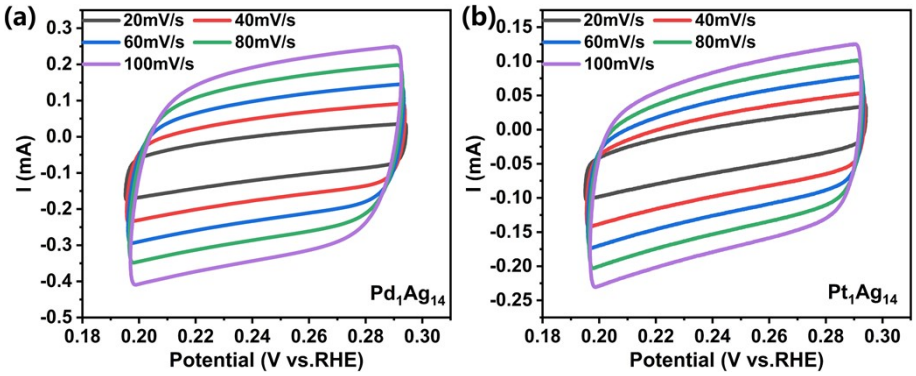


**Fig. S16** CV curves at various scan rates (from 20 to 100 mV $s^{-1}$) of (a) **$Pd_1Ag_{14}$/C** and (b) **$Pt_1Ag_{14}$/C**.

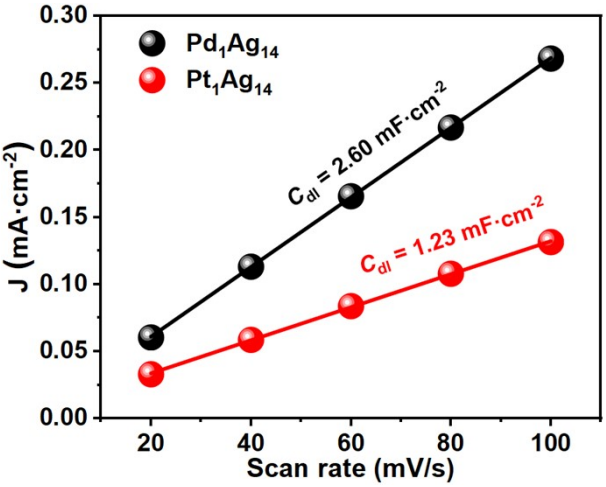


**Fig. S17** The comparison of electrochemical double layer capacitance over **$Pd_1Ag_{14}$/C** (black line) and **$Pt_1Ag_{14}$/C** (red line).

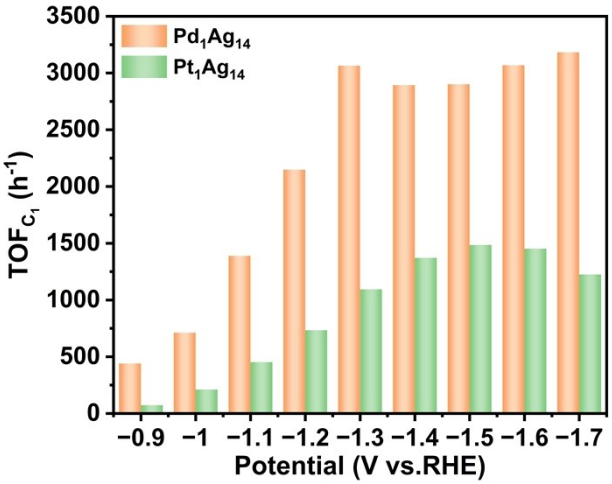


**Fig. S18** The turnover frequency of $C_1$ products was obtained from **$Pd_1Ag_{14}$/C** and **$Pt_1Ag_{14}$/C**.

## Section 2. Supporting Tables

**Table S1.** The crystal structure parameters for **$Pt_1Ag_{14}$** nanocluster.

| | |
|---|---|
| Empirical formula | $C_{183}H_{177}Ag_{14}O_{21}P_7PtS_6$ |
| Formula weight | 4826.66 |
| Temperature/K | 120 |
| Crystal system | triclinic |
| Space group | *P*-1 |
| a/Å | 19.411 |
| b/Å | 20.798 |
| c/Å | 27.800 |
| α/° | 81.778 |
| β/° | 75.137 |
| γ/° | 83.738 |
| Volume/Å$^3$ | 10706 |
| Z | 2 |
| $\rho_{calc}$g/cm$^3$ | 1.497 |
| μ/mm$^{-1}$ | 2.062 |
| F(000) | 4760.0 |
| Crystal size/mm$^3$ | 0.113 × 0.091 × 0.086 |
| Radiation | Mo Kα (λ = 0.71073) |
| 2Θ range for data collection/° | 3.968 to 50.852 |
| Reflections collected | 38476 |
| Independent reflections | 36476 [$R_{int}$ = 0.172, $R_{sigma}$ = 0.3432] |
| Data/restraints/parameters | 36476/2932/1786 |
| Goodness-of-fit on $F^2$ | 0.862 |
| Final R indexes [I>=2σ (I)] | $R_1$ = 0.0966, $wR_2$ = 0.2076 |
| Final R indexes [all data] | $R_1$ = 0.2266, $wR_2$ = 0.2467 |
| Largest diff. peak/hole / e Å$^{-3}$ | 2.01/-1.75 |

**Table S2.** The data of Bader charge analysis for the $Pd_1Ag_{14}$ nanocluster.

| Atom labels | X | Y | Z | Charge | Min dist | Atomic vol |
|---|---|---|---|---|---|---|
| Pd1 | 15.00522 | 14.55735 | 14.81242 | 10.2563 | 1.25858 | 16.47431 |
| Ag1 | 15.85143 | 13.30881 | 12.46315 | 10.90304 | 1.10907 | 23.7125 |
| Ag2 | 15.8037 | 17.22564 | 15.15252 | 10.94374 | 1.11189 | 25.67444 |
| Ag3 | 16.99509 | 12.58974 | 15.08084 | 10.94768 | 1.1277 | 25.81931 |
| Ag4 | 14.17812 | 11.88546 | 14.47345 | 10.94708 | 1.12371 | 25.72403 |
| Ag5-exposed | 15.63585 | 14.66397 | 19.43827 | 10.73495 | 1.11374 | 40.42889 |
| Ag6 | 13.09641 | 14.10876 | 12.82603 | 10.90697 | 1.08516 | 23.76403 |
| Ag7 | 17.60724 | 15.20712 | 13.92528 | 10.93853 | 1.11294 | 25.77653 |
| Ag8 | 14.11554 | 15.81204 | 17.14969 | 10.9014 | 1.11588 | 23.85542 |
| Ag9 | 15.1527 | 16.11552 | 12.50382 | 10.90596 | 1.0802 | 23.8875 |
| Ag10 | 12.41901 | 13.8924 | 15.68823 | 10.9395 | 1.09559 | 25.39639 |
| Ag11 | 13.02603 | 16.55244 | 14.53949 | 10.94025 | 1.11494 | 25.83097 |
| Ag12 | 16.93335 | 15.03114 | 16.77694 | 10.90621 | 1.09207 | 23.66681 |
| Ag13 | 14.86863 | 12.9615 | 17.10776 | 10.90016 | 1.10375 | 23.66292 |
| Ag14 | 14.31843 | 14.46171 | 9.64894 | 10.75393 | 1.15533 | 22.38931 |

**Table S3.** The data of Bader charge analysis for the $Pt_1Ag_{14}$ nanocluster.

| Atom labels | X | Y | Z | Charge | Min dist | Atomic vol |
|---|---|---|---|---|---|---|
| Pt1 | 14.47944 | 14.16897 | 14.83601 | 10.51758 | 1.28697 | 18.58694 |
| Ag1 | 14.31372 | 13.78587 | 9.68065 | 10.71844 | 1.14555 | 22.33875 |
| Ag2 | 13.14885 | 12.91476 | 12.71515 | 10.87907 | 1.08131 | 23.41792 |
| Ag3 | 12.4011 | 12.41415 | 15.5274 | 10.92059 | 1.08051 | 25.29236 |
| Ag4 | 11.84778 | 15.02997 | 14.34521 | 10.92461 | 1.09247 | 25.21653 |
| Ag5 | 14.08242 | 15.64476 | 12.48877 | 10.88545 | 1.08549 | 23.47917 |
| Ag6 | 14.98434 | 11.41224 | 14.50817 | 10.93531 | 1.13317 | 25.45958 |
| Ag7 | 15.98352 | 13.46559 | 12.59125 | 10.89175 | 1.10396 | 23.3975 |
| Ag8 | 16.54869 | 15.93915 | 14.13223 | 10.92096 | 1.08579 | 25.47028 |
| Ag9 | 17.09769 | 13.27467 | 15.31436 | 10.92224 | 1.11704 | 25.59667 |
| Ag10 | 15.85494 | 15.4278 | 16.92779 | 10.87515 | 1.09357 | 23.59 |
| Ag11 | 14.84559 | 12.66357 | 17.16631 | 10.87877 | 1.1161 | 23.29736 |
| Ag12 | 12.95172 | 14.91417 | 17.05837 | 10.88674 | 1.09344 | 23.50444 |
| Ag13-exposed | 14.64354 | 14.51889 | 19.4901 | 10.70281 | 1.10356 | 39.79306 |
| Ag14 | 13.97097 | 16.91667 | 15.13859 | 10.93361 | 1.11706 | 25.41097 |